Nuclear Science and Techniques (2023) 34:27
https://doi.org/10.1007/s41365-023-01179-2

# Study on the effect of thermal deformation on the liquid seal of high-temperature molten salt pump in molten salt reactor

Xing-Chao Shen[1,2] · Yuan Fu[1] · Jian-Yu Zhang[1]

Received: 27 September 2022 / Revised: 30 November 2022 / Accepted: 2 December 2022 / Published online: 25 February 2023


## Abstract

The high-temperature molten salt pump is the core equipment in a molten salt reactor that drives the flow of the molten salt coolant. Rotor stability is key to the continuous and reliable operation of the molten salt pump, and the liquid seal at the wear ring can affect the dynamic characteristics of the rotor system. When the molten salt pump is operated in the high-temperature molten salt medium, thermal deformation of the submerged parts inevitably occurs, changing clearance between the stator and rotor, affecting the leakage and dynamic characteristics of the seal. In this study, the seal leakage, seal dynamic characteristics, and rotor system dynamic characteristics are simulated and analyzed using finite element simulation software based on two cases of considering the effect of seal thermal deformation effect or not. The results show a significant difference in the leakage characteristics and dynamic characteristics of the seal obtained by considering the effect of seal thermal deformation and neglecting the effect of thermal deformation. The leakage flow rate decreases, and the first-order critical speed of the seal-bearing-rotor system decrease after considering the seal's thermal deformation.

**Keywords** High-temperature molten salt pump · Seal thermal deformation · Leakage characteristics · Seal dynamic characteristics · Critical speed

## 1 Introduction

The thorium-based molten salt reactor (TMSR) [1] nuclear energy system is one of the strategically advanced research projects of the Chinese Academy of Sciences that uses molten salt as the reactor coolant. The high-temperature molten salt pump is essential for the molten salt reactor and is responsible for driving the circulating flow of the molten salt coolant. Its design temperature is 700 °C, at a micro-positive pressure, and the material used is austenitic stainless steel. As shown in Fig. 1, the high-temperature molten salt pump is a vertical cantilever-submerged centrifugal pump. The motor is mounted on top, and two groups of bearings support the entire shaft system component. The molten salt level is two-thirds of the height of the pump tank, and the impeller is fully immersed in the molten salt. The liquid molten salt from the downside is transported to the pumping chamber due to the centrifugal force generated by impeller rotation. However, the presence of clearance at the wear ring can cause the liquid in the pumping chamber to backflow resulting in a leakage in the pump. The presence of the liquid seal at the wear ring generates liquid stiffness and damping, which has an impact on the swirl motion and dynamic characteristics of the rotating shaft. The size of the clearance at the wear ring is the main cause of leakage, which affects the lift, flow, and efficiency of the molten salt pump. Therefore, the design and calculation of clearance are critical for main nuclear pumps. However, under actual operating conditions, the seal is thermally deformed by the high-temperature molten salt, which changes the dynamic characteristics of the seal, causing different effects on the leakage and the stability of the rotor system.

This work was supported by the Strategic Pilot Technology Chinese Academy of Sciences (No. XDA02010500).

✉ Yuan Fu
fuyuan@sinap.ac.cn

✉ Jian-Yu Zhang
zhangjianyu@sinap.ac.cn

[1] Shanghai Institute of Applied Physics, Chinese Academy of Sciences, Shanghai 201800, China

[2] University of Chinese Academy of Sciences, Beijing 100049, China

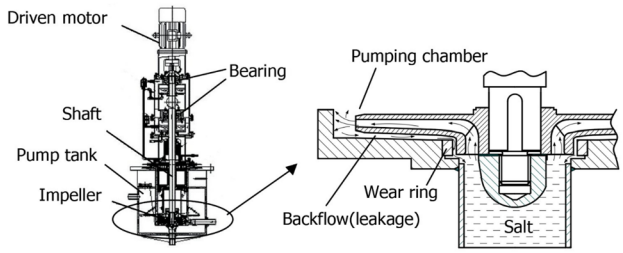


**Fig. 1** Model diagram of high-temperature molten salt pump

The pressure field in the seal can generate a force induced by the fluid. In some cases, the effect of this force can become significant, significantly affecting the overall dynamic characteristics of the pump. Thus, the fluid forces applied to the rotor by the seal during the operation of the molten salt pump must be accurately quantified to effectively predict the dynamic behavior of the rotor [2]. Black [3] used the short bearing theory to derive an equation that calculates the seal power coefficient and then explored the effect of hydraulic pressure in the ring seal on the rotor vibration of the centrifugal pump. Childs et al. [4] derived an expression for the dynamic coefficient of the high-pressure annular seal of a multistage centrifugal pump based on the Hirs lubrication equation. They discussed the fluid field in the seal cavity in detail. Moore et al. [5] used a pressure-based computational fluid dynamics (CFD) program to calculate the flow field and fluid dynamics parameters of a slotted liquid seal. They then compared the measured values obtained using a 3D laser Doppler anemometer with the calculated values. Untaroiu et al. [6] analyzed and calculated the fluid-induced forces acting on a rotor using 3D computational hydrodynamics. They then expressed it in terms of the equivalent linearized stiffness, damping, and fluid inertia coefficients. These kinetic coefficients were used to predict the rotordynamics behavior of industrial pumps, and the calculated values were compared with the vibration characteristics measured during the pump house tests. The final results showed the high reliability of CFD. DaqiqShirazi et al. [7] used a combination of numerical simulations and experiments to study the effect of wear ring clearance on the performance of centrifugal pumps. They found that when the clearance increased, the internal leakage increased, and the pump efficiency decreased significantly. In the molten salt pump study, Shao et al. [8] tested the external characteristics by using water as the experimental medium and verified the correctness of the numerical simulation model by comparison. They theoretically analyzed the performance curve of the molten salt pump and studied the relationship among fluid viscosity, external characteristics, and flow field from the perspective of energy loss analysis. Wang et al. [9] made geometric improvements to the molten salt pump using numerical and experimental methods. The results indicated that the hydraulic efficiency of the modified molten salt pump was improved, and the pressure fluctuation and vibration intensity were reduced. He [10] studied a centrifugal molten salt pump using numerical simulation. She calculated the external characteristics, internal flow field, force, and deformation of the rotor parts of the molten salt pump under different radial clearances of the port ring and different axial lengths of the wear ring. Finally, she analyzed the effects of different radial clearances and axial lengths of the ring on the performance of the molten salt pump and the force on the rotor parts. Hu et al. [11] used computational fluid dynamics techniques to simulate the flow in the sealing zone and analyzed the rotordynamics coefficients. They investigated the rotordynamic characteristics of the molten salt pump with and without the liquid seal and showed that the first-order critical speed of the rotor increased under the condition of the liquid seal. Concerning the research on the thermal deformation of the seal, Subramanian et al. [12, 13] analyzed the effect of centrifugal and thermal radial growth of the gas turbine seal on the amount of leakage by considering only the rotor deformation—without considering the stator deformation. They found that radial growth and leakage flow changed significantly with increasing radius and explored the effect of combined centrifugal and thermal radial growth on the rotordynamic characteristics of the seal. Currently, most research on molten salt pumps focuses on hydraulic and structural characteristics [14–16], and little research is related to the thermal deformation of the seal of the molten salt pump. Research on the influence of thermal deformation on seal leakage and dynamic characteristics is notable for improving the efficiency and reliability of molten salt pumps.

This study uses numerical simulation to calculate the seal leakage and dynamic characteristics. CFD software was used for two cases of the annular seal of the molten salt pump by considering and ignoring thermal deformation. On this basis, the obtained seal dynamic characteristic coefficients are applied to the rotor, and the critical speed of the rotor system is calculated using the finite element software. Moreover, this study compares the numerical calculation results obtained from the two cases to study the effect of thermal deformation on the seal, explore the dynamics of the seal under actual working conditions, and provide a reference for further improving the stability of high-temperature molten salt pumps.

## 2 Analytical model

The stator and rotor of the molten salt pump shaft system contact the high-temperature molten salt, and both undergo thermal deformation. However, the stator hole part is much

more constrained and influenced by the shape than the rotor shaft part; thus, the radial thermal deformation of the hole part is smaller than that of the shaft part, and the seal clearance significantly changes after high-temperature thermal deformation. For high-temperature equipment such as molten salt pumps designed for 700 °C, the clearance change must be considered to fulfill the analysis requirements for the actual operating conditions. The calculation formula for the clearance $C_T$ after seal thermal deformation is:

$$C_T = C + (U_t - U_r)/2, \tag{1}$$

where $C$ is the original clearance, $U_t$ is the stator radial thermal deformation, and $U_r$ is the rotor radial thermal deformation.

## 2.1 Seal dynamic model

In the dynamic model shown in Fig. 2, the pump shaft, while rotating on itself at speed $\omega$, also rotates around the geometric center at speed $\Omega$, where the eccentricity is $e$. For the rotating film of liquid molten salt in the clearance, it generates a fluid excitation force that can be expressed with reference to the dynamic pressure-bearing oil film force as follows:

$$-\begin{bmatrix} F_x \\ F_y \end{bmatrix} = \begin{bmatrix} K_{xx} & K_{xy} \\ K_{yx} & K_{yy} \end{bmatrix}\begin{bmatrix} X \\ Y \end{bmatrix} + \begin{bmatrix} C_{xx} & C_{xy} \\ C_{yx} & C_{yy} \end{bmatrix}\begin{bmatrix} \dot{X} \\ \dot{Y} \end{bmatrix} + \begin{bmatrix} M_{xx} & M_{xy} \\ M_{yx} & M_{yy} \end{bmatrix}\begin{bmatrix} \ddot{X} \\ \ddot{Y} \end{bmatrix} \tag{2}$$

When the pump shaft makes a small eccentric distance swirl motion in the seal cavity, the anisotropic effects in the seal system can be ignored. Then, the seal dynamic characteristic coefficients in the aforementioned equation have the following relationship [17]: $K_{xx}=K_{yy}=K$, $K_{xy}=-K_{yx}=k$, $C_{xx}=C_{yy}=C$, $C_{xy}=-C_{yx}=c$, $M_{xx}=M_{yy}=M$, $M_{xy}=-M_{yx}=m$. Therefore, the seal dynamics model of Eq. (2) can be simplified as follows:

$$-\begin{bmatrix} F_x \\ F_y \end{bmatrix} = \begin{bmatrix} K & k \\ -k & K \end{bmatrix}\begin{bmatrix} X \\ Y \end{bmatrix} + \begin{bmatrix} C & c \\ -c & C \end{bmatrix}\begin{bmatrix} \dot{X} \\ \dot{Y} \end{bmatrix} + \begin{bmatrix} M & m \\ -m & M \end{bmatrix}\begin{bmatrix} \ddot{X} \\ \ddot{Y} \end{bmatrix} \tag{3}$$

The dynamic coefficients of the seal in Eqs. (2) and (3) are as follows: $K_{xx}$, $K_{yy}$, and $K$ represent the direct stiffness of the system; $K_{xy}$, $K_{yx}$, and $k$ represent the cross-coupled stiffness of the system; $C_{xx}$, $C_{yy}$, and $C$ represent the direct damping of the system; $C_{xy}$, $C_{yx}$, and $c$ represent the cross-coupled damping of the system; $M_{xx}$, $M_{yy}$, and $M$ represent the direct mass of the system; and $M_{xy}$, $M_{yx}$, and $m$ represent the cross-coupled mass of the system.

In order to predict the seal performance of the clearance of the molten salt pump and to obtain the six seal dynamic coefficients aforementioned, this study used a relative rotational coordinate system solution for the calculation, which is easier to solve and requires less computationally than the absolute stationary coordinate system. This solution transforms the transient problem into a quasi-stable problem (Fig. 3a, b). The liquid molten salt in the clearance is treated as a rotational domain, where the region rotates around the stator center at rotational speed $\Omega$; the stator surface reverses at rotational speed $\Omega$, and the rotor surface rotates around the rotor center at rotational speed $\omega - \Omega$. When the rotor performs a small swirl motion, the radial and tangential forces [18] can be obtained from Eq. (3) as follows:

$$\frac{F_r}{e} = \frac{F_x}{e} = -K - c\Omega + M\Omega^2, \tag{4}$$

$$\frac{F_t}{e} = \frac{F_y}{e} = k - C\Omega - m\Omega^2. \tag{5}$$

In this study, the eccentricity distance was selected as 10% of the radial clearance, and Moore et al. [5] verified the accuracy of this value in simulating small trajectory eddy motion. Next, CFD was used to solve the molten salt flow field, which can obtain the relationship equation of

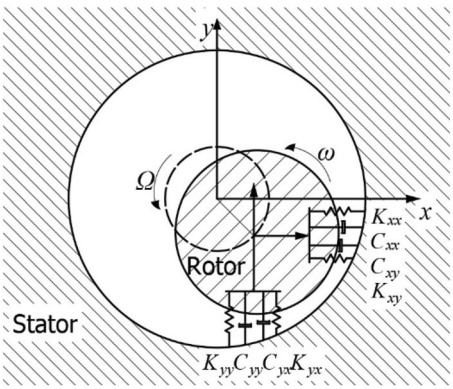


**Fig. 2** Dynamic modeling of the seal

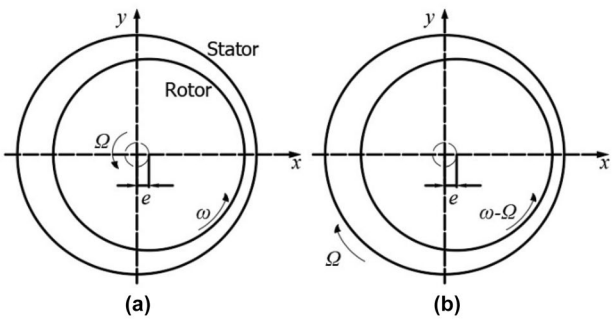


**Fig. 3** Coordinate system selection. **a** Absolute fixed coordinate system; **b** rotating relative coordinate system

multigroup swirl velocity Ω with radial force $F_x$ and tangential force $F_y$ and then obtain six seal dynamics characteristic coefficients by curve fitting against Eqs. (4) and (5). If the direct stiffness $K$ is negative, the liquid film creates a force that intensifies rotor eccentricity. The cross-coupled stiffness $k$ and direct damping $C$ are related to rotor stability. The cross-coupled stiffness $k$ is the source that promotes the increase in rotor swirl, and direct damping $C$ is the source that suppresses the increase in rotor swirl. For the molten salt flow field in the clearance, the stability of the seal can be evaluated by the effective damping factor $C_{\text{eff}}$. The effective damping factor represents whether the value of the destabilization term in the seal system exceeds the damping amount and can be used to determine whether the seal negatively affects the stability of the rotor system.

## 2.2 Fluid calculation model

### 2.2.1 Mathematical model

In the seal clearance, the liquid molten salt is affected by the swirl and spin of the pump shaft, which creates intense motion. In this study, the CFD numerical method and the standard $k-\varepsilon$ turbulence model were used to solve the molten salt flow field. The seal is in the submerged part of the molten salt pump, and the operating temperature is considered as a constant; thus, the energy conservation equation is not considered in the control equation. The detailed equations are as follows:

continuity equation:

$$\frac{\partial \rho}{\partial t}+\frac{\partial}{\partial x_i}(\rho u_i)=0, \tag{6}$$

momentum equation:

$$\frac{\partial}{\partial x_i}(\rho u_i)+\frac{\partial}{\partial x_i}(\rho u_i u_j)=-\frac{\partial p}{\partial x_i}+\frac{\partial}{\partial x_j}\left[\mu\frac{\partial u_i}{\partial x_j}-\rho\overline{u_i' u_j'}\right]+S_i, \tag{7}$$

$k$ equation:

$$\frac{\partial(\rho k)}{\partial t}+\frac{\partial(\rho k u_i)}{\partial x_i}=\frac{\partial}{\partial x_j}\left[\left(\mu+\frac{\mu_t}{\sigma_k}\right)\frac{\partial k}{\partial x_j}\right]+G_k-\rho\varepsilon, \tag{8}$$

$\varepsilon$ equation:

$$\frac{\partial(\rho\varepsilon)}{\partial t}+\frac{\partial(\rho\varepsilon u_i)}{\partial x_i}=\frac{\partial}{\partial x_j}\left[\left(\mu+\frac{\mu_t}{\sigma_\varepsilon}\right)\frac{\partial \varepsilon}{\partial x_j}\right]+\frac{C_{1\varepsilon}\varepsilon}{k}G_k-C_{2\varepsilon}\rho\frac{\varepsilon^2}{k}, \tag{9}$$

where $\rho$ is the fluid density, $u$ is the velocity, $p$ is the pressure, $t$ is the time, $x$ is the space coordinate, $\mu$ is the dynamical viscosity, $S$ is the source term, $G_k$ is the turbulent energy term generated by the mean velocity gradient, $C_{1\varepsilon}$ and $C_{2\varepsilon}$ are the constant terms of the equation, $\sigma_k$ and $\sigma_\varepsilon$ are the turbulent Prandtl numbers of the turbulent energy $k$ and dissipation rate $\varepsilon$, and $\mu_t$ is the turbulent viscosity.

### 2.2.2 Boundary conditions and solution method

The molten salt medium in the pump was LiF–NaF–KF molten salt (FLiNaK) with molar ratios of 46.5%, 11.5%, and 42%, and density $\rho=2.02$ g/cm$^3$ and kinematic viscosity $\mu=0.0029$ Pa/s at the operating temperature of 700 °C. The selected ring seal dimensions are as follows: diameter $D=100$ mm, clearance $C=0.5$ mm, and seal length $L=40$ mm. In ANSYS Fluent, this study set the shaft speed to 1500 rpm, the total pressure to 0.1 MPa at the inlet of the calculation domain, and the static pressure to zero at the outlet. The rotor and seal surface were standard wall conditions with no-slip velocity conditions and the adiabatic wall. The model was solved by placing it in a relatively rotating coordinate system, where the rotational speed of the rotating coordinate system was the swirl speed Ω. The seal surface was set as a rotating wall surface with a reverse swirl speed of $-\Omega$. The rotating shaft surface was set as a rotating wall surface with a speed $\omega-\Omega$ rotating around the rotor center. The solver was selected as a separate implicit solver, and the finite volume method was used to discretize the control equations. The continuity and momentum equations were in the discrete format in the second-order windward format, and the turbulent kinetic energy and dissipation rate equations were in the first-order windward format. The pressure–velocity coupling equation was solved using the SIMPLE algorithm, and the solution was judged to converge when the residuals of all equations were less than $1\times10^{-5}$, at which point the inlet and outlet mass flow rates were equal. In order to fit the equations for the radial and tangential forces and obtain the seal dynamics characteristic coefficients, this study had to select at least three different vortex velocities Ω for calculation. Next, to improve the calculation accuracy, this study selected seven swirl velocities for calculation.

## 2.3 Model reliability checking

### 2.3.1 Computational model validation

Aimed at checking the correctness of the seal dynamic model and ANSYS Fluent numerical simulation, this study used the aforementioned method to numerically calculate the experimental model of the annular seal of Lindsey and Childs [19]. The results of the numerical simulation were compared with the experimental test values and theoretical values of Lindsey to check the reliability of the method. The schematic of the experimental model is shown in Fig. 4, where the rotor eccentricity is 10%; seal length, $L=13.13$ mm; clearance, $C=0.076$ mm; rotor shaft diameter, $d=76.2$ mm; liquid

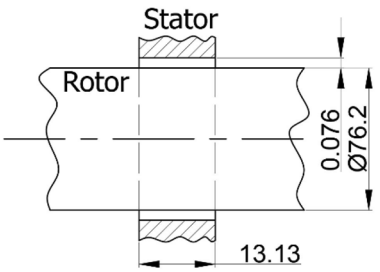


**Fig. 4** Experimental model

density, $\rho = 986.7$ kg/m$^3$; and liquid dynamic viscosity, $\mu = 5.17 \times 10^{-4}$ Pa s. $\Delta P$ is the differential pressure between the inlet and outlet, calculated numerically for three values: 1.38, 2.41, and 3.45 MPa.

As shown in Fig. 5, this study compared the experimental test values, theoretically calculated values, and numerically calculated values of leakage and the direct stiffness coefficient based on Lindsey's experimental model. The results show that the numerical calculation results are between those of the other two and are closer to the experimental values, indicating that the numerical method is reliable.

### 2.3.2 Grid independence verification

In this study, seven meshing options were obtained with meshing software, calculated according to the boundary conditions in Sect. 2.2.2, and the mesh independence verification was performed with the outlet leakage as the objective function. As shown in Fig. 6, when the grid number reached 288,000, the relative error of leakage did not exceed 0.1%, and the effect of the change in grid number on the CFD simulation was considered negligible. Finally, computational accuracy and computational cost were considered, and the option with a grid number of 288,000 was selected for the numerical simulation.

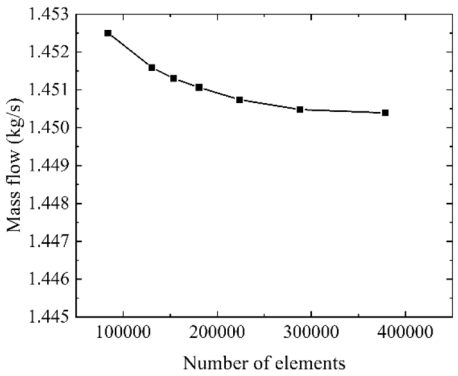


**Fig. 6** Leakage rate versus number of grid

## 2.4 Rotordynamics model of the shaft system

The inhomogeneous pressure field created from the molten salt flow in the seal clearance can have an impact on the dynamic characteristics of the pump shaft rotor. Therefore, when analyzing the rotordynamics of the pump shaft, it is necessary to consider not only the stiffness provided at the mechanical bearing but also the added mass, added stiffness, and added damping generated from the seal. The effect on the pump shaft at the seal can be simplified as an elastic support unit for rotordynamic calculations. The gyroscopic effect occurs when the rotor rotates; thus, the differential equation for the rotordynamic equation is:

$$[M]\{\ddot{U}\} + [C + G]\{\dot{U}\} + [K]\{U\} = \{F\}, \tag{10}$$

where $M$ is the mass matrix, $C$ is the damping matrix, $G$ is the gyroscopic matrix, $K$ is the stiffness matrix, $U$ is the generalized coordinate vector of the rotor system, and $F$ is the external force acting on the rotor.

To investigate the seal's influence on the rotordynamics of the molten salt pump and compare the difference between considering and neglecting the thermal deformation of the seal,

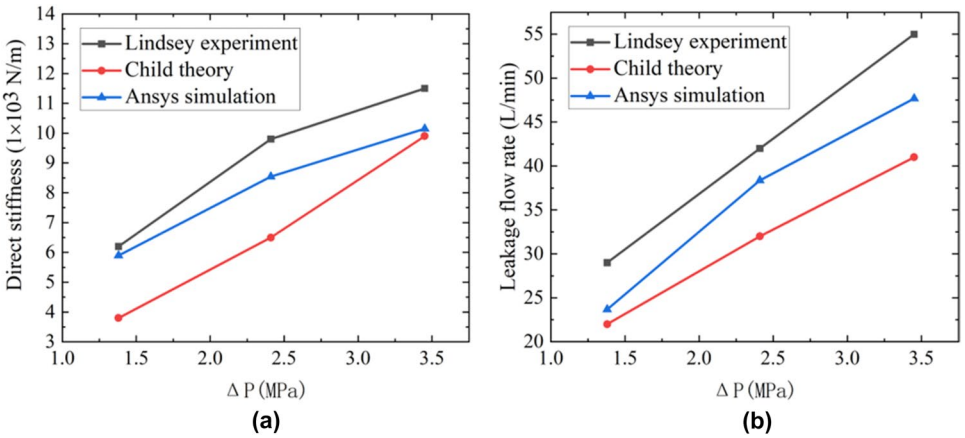


**Fig. 5** Computational model validation. **a** Leakage comparison; **b** comparison of direct stiffness coefficients

this study used the ANSYS Workbench to calculate the critical speed of the rotor system. The pump shaft is the cantilever type, supported by two mechanical bearings on the upper side and affected by the seal liquid film at the impeller. The mechanical bearings provided a direct stiffness of $8\times10^7$ N/m. The stiffness and damping provided to the rotating shaft at the seal are inputs from the seal dynamic characteristic coefficients this study has obtained. The calculation results of three cases, bearing-rotor system critical speed, seal (neglecting thermal deformation)-bearing-rotor system critical speed, and seal (considering thermal deformation)-bearing-rotor system critical speed, were compared and analyzed. Figure 7 shows the finite element model of the rotor system.

## 3 Result and discussion

### 3.1 Analysis of calculation result of thermal deformation

Xu [20] and Ni [21] concluded in an experimental study of hole-shaft thermal deformation that the radial heat deformation of shaft parts can be estimated by the traditional formula. However, the traditional formula is not applicable for radial heat deformation of the hole parts. Because the coefficient of thermal expansion of austenitic stainless steel is larger than that of ordinary carbon steel, this study considered thermal deformation from the perspective of conservativeness. Both the stator and rotor at the seal in the high-temperature molten salt pump are regarded as free thermal expansion, and the radial thermal expansion coefficient of the rotor can be directly adopted from the linear expansion coefficient of steel at 700 °C ($13.79\times10^{-6}$ °C$^{-1}$). The radial thermal expansion coefficient of the stator hole is smaller than that of the rotor shaft because there is more binding force on the molecular thermal movement of the inner diameter than the outer diameter of the hole. Ni [21] measured that the thermal expansion coefficients of the shaft and hole of 100 mm were $8.2\times10^{-6}$ °C$^{-1}$ and $6.4\times10^{-6}$ °C$^{-1}$ in −20 to 80 °C experiments and demonstrated the difference in thermal deformation of the shaft and hole. Owing to the limitations of experimental conditions, no experimental data on the radial thermal expansion coefficient of the hole at 700 °C were available. Therefore, this study refers to the different ratios of the radial thermal expansion coefficient of the hole and shaft from the experiment of Ni at low temperature and uses the radial thermal expansion coefficient of the hole as $10.76\times10^{-6}$ °C$^{-1}$. When the seal clearance is 0.5 mm, the amount of change in the clearance after considering thermal expansion can be obtained according to Eq. (1).

As shown in Table 1, after the seal is affected by the high-temperature molten salt, the change in the clearance is obvious, with a 20.24% difference between the two, and the finite element simulation software cannot reflect this experimental difference. In the experiment on the measurement of thermal deformation of hollow cylindrical parts, Miao et al. [22] found a defect: the thermal expansion characteristics of the parts do not match reality when using ANSYS Workbench thermal analysis. Different seal clearances can have different effects on seal leakage and dynamics.

### 3.2 Analysis of calculation result of leakage

Figure 8 shows the variation in the leakage flow rate at the molten salt pump ring with the rotational speed for the two cases of considering and neglecting the thermal deformation. In both cases, the leakage flow rate decreases as the pump shaft speed increases. When the pump shaft speed is 500–10,000 rpm, the leakage flow rate of the seal considering thermal deformation is always lower than that when thermal deformation is neglected. Focusing on when the pump speed is 1500 rpm, the leakage flow rate is 1.4505 kg/s by ignoring thermal deformation, whereas the leakage amount is 0.89363 kg/s by considering thermal deformation. The difference between the two values was 0.5542 kg/s, and the difference ratio was 38.2%. The main reason for the reduction in seal leakage is that the clearance of the seal is significantly smaller after considering thermal deformation; thus, the mass flow rate of the molten salt in the return flow is also reduced.

**Table 1** Calculation of clearance change

| | Neglecting thermal deformation | Finite element | Reference experimental value |
|---|---|---|---|
| Clearance size (mm) | 0.5 | 0.5005 | 0.3988 |
| Change amount (mm) | 0 | 0.0048 | 0.1012 |
| Change ratio | 0% | 0.96% | 20.24% |

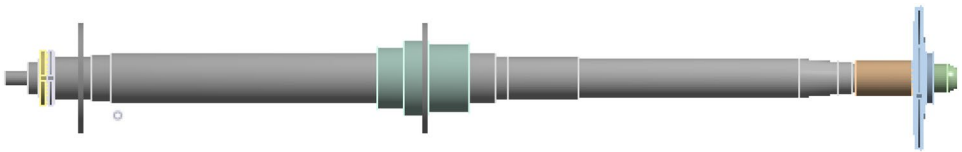

**Fig. 7** (Color online) Calculation model of critical speed

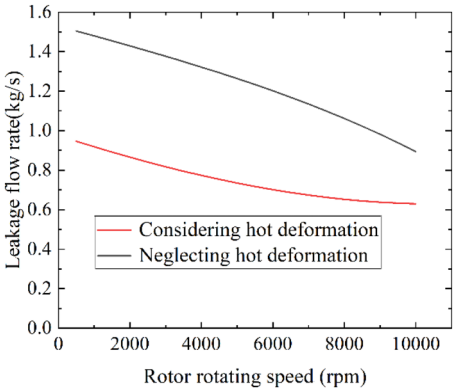


**Fig. 8** Leakage versus rotational speed

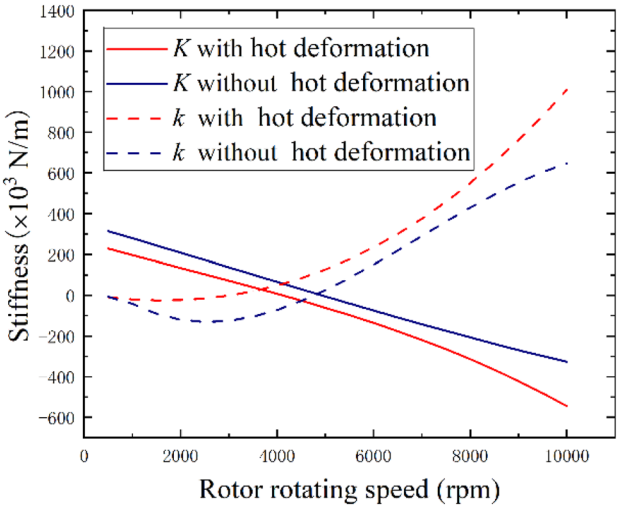


**Fig. 10** (Color online) Added stiffness versus rotational speed

### 3.3 Analysis of seal film pressure

As shown in Fig. 9, the circumferential pressure distribution is obtained by considering and neglecting the thermal deformation at half the shaft length of the annular seal at 1500 rpm. The centers of both pressure characteristic ellipses are off to the right, representing positive direct stiffness from both seals. In the pressure distribution diagram, the pressure difference between the left and right sides obtained by neglecting thermal deformation is larger than that obtained by considering thermal deformation; therefore, the support counterforce produced by neglecting the thermal deformation on the eccentricity of the rotating shaft is larger.

### 3.4 Analysis of seal dynamic characteristic

Figure 10 shows the variation curves of the direct stiffness $K$ and cross-coupled stiffness $k$ of the seal with rotational speed for both cases, considering and neglecting the thermal deformation. The direct stiffness $K$ decreases as shaft speed increases in both cases, is positive in the low-speed region, and decreases to a negative value in the high-speed region. The main reason for this phenomenon is that when the speed is high, the pump shaft will produce a large shear motion with the molten salt fluid in the ring; thus, the axial flow of molten salt in the ring is reduced, and the seal clearance is more likely to produce a negative direct stiffness. The direct stiffness obtained by considering thermal deformation is smaller than that obtained by neglecting thermal deformation. The cross-coupled stiffness $k$ increases with an increase in the pump shaft speed in both cases; thus, the sources promoting the intensification of the rotor swirl also increase. The cross-coupled stiffness obtained by considering the seal's thermal deformation is larger than that obtained by neglecting thermal deformation.

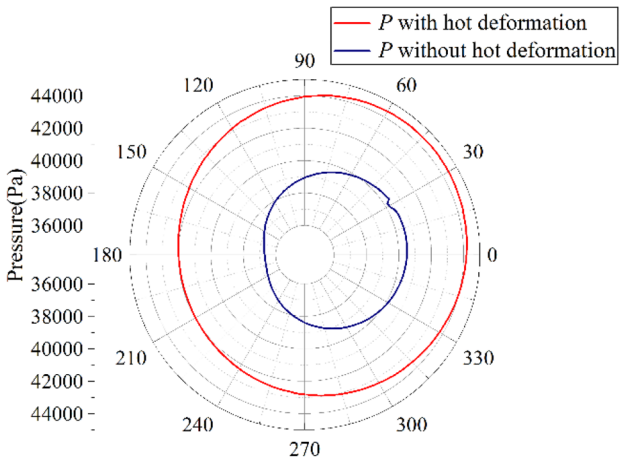


**Fig. 9** (Color online) Circumferential pressure distribution

As shown in Fig. 11a, direct damping $C$ and cross-coupled damping $c$ increase as speed increases in both cases of considering and neglecting thermal deformation, where the increase in direct damping can play a role in suppressing rotor instability. The direct damping obtained by considering thermal deformation is greater than that obtained by neglecting thermal deformation, and the two values become similar as the speed increases.

As shown in Fig. 11b, the direct added mass $M$ does not produce a significant change as the speed increases. The direct added mass obtained by considering thermal deformation is smaller than that obtained by neglecting thermal deformation, which is due to the reduction in the molten salt in the clearance after considering thermal deformation. Because the cross-coupled added mass $m$ is almost zero, its effect is not considered.

At 1500 rpm, this study compared the seal dynamic characteristic coefficients obtained by considering and

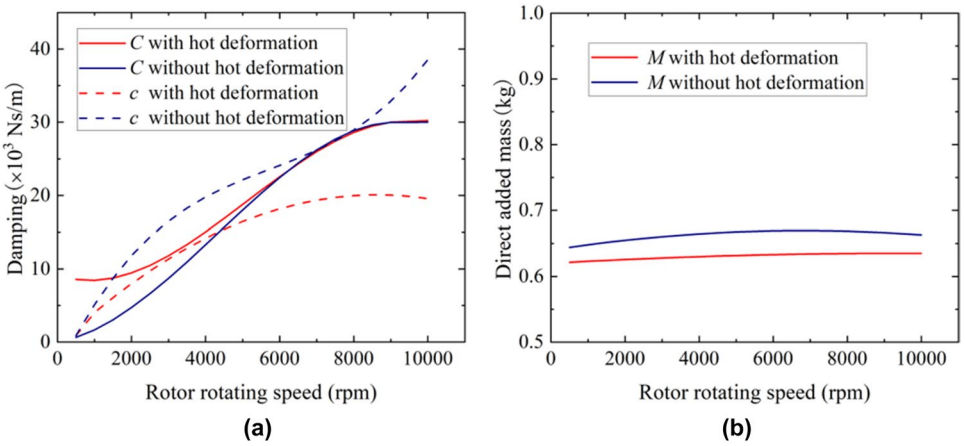


**Fig. 11** (Color online) Added damping and added mass. **a** Added damping versus rotational speed; **b** added mass versus rotational speed

**Table 2** Comparison of seal dynamic characteristics coefficients

| | Considering thermal deformation | Neglecting thermal deformation | Difference ratio (%) |
|---|---|---|---|
| $K$ ($\times 10^3$ N/m) | 169.1 | 238.4 | 29.1 |
| $k$ ($\times 10^3$ N/m) | − 24.32 | − 86.59 | 73.9 |
| $C$ ($\times 10^3$ Ns/m) | 8.739 | 2.382 | 266.9 |
| $c$ ($\times 10^3$ Ns/m) | 8.319 | 8.674 | 4.1 |
| $M$ (kg) | 0.6285 | 0.662 | 5.1 |

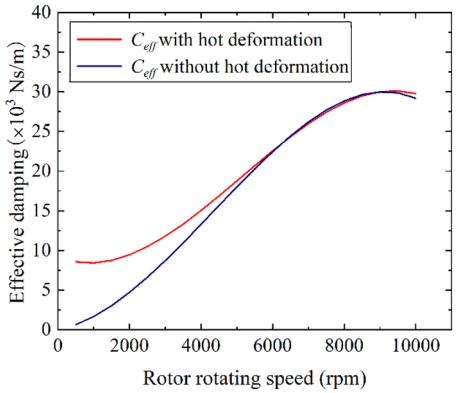


**Fig. 12** (Color online) Added damping versus rotational speed

neglecting thermal deformation. The specific values are listed in Table 2. The difference ratio (neglecting thermal deformation as a benchmark) is as high as 266.9% for direct damping and 73.9% for cross-coupled stiffness, and different direct damping and cross-coupled stiffness make the liquid film exhibit various stability. The direct stiffness difference ratio is 29.1%; thus, the influence of the liquid film on the rotating shaft support also differs. Both the cross-coupled damping and directly added mass exhibit a slight difference ratio. Crucially, different seal dynamic characteristic coefficients have different effects on the critical speed and rotor stability in the subsequent rotordynamics.

### 3.5 Analysis of seal stability

The aforementioned works obtained dynamic characteristic coefficients of the molten salt pump in the speed range of 500–10,000 rpm, and the seal stability can be evaluated by the effective damping coefficient ($C_{\text{eff}} = C - k/\omega$). When $C_{\text{eff}}$ is greater than 0, which means the seal is stable; otherwise, it means the seal is unstable. As shown in Fig. 12, the effective damping coefficient shows a trend of increasing and then decreasing with increasing rotational speed for both cases of the seal by considering and neglecting thermal deformation. $C_{\text{eff}}$ is a positive value throughout the speed region, which indicates that the value of the destabilization term in the system is not greater than the damping amount, although the cross-coupled stiffness increases; thus, the seal still exhibits a stable effect. In the low-speed region, the effective damping coefficient obtained by considering thermal deformation is larger than that obtained by neglecting thermal deformation; thus, it exhibits stability better. As the speed increases, the difference between the two values becomes insignificant. Therefore, to improve the matching of the actual working conditions and the accuracy of the seal dynamics calculation, the designs of the seal of a high-temperature molten salt pump should consider the influence of the thermal deformation of the seal.

### 3.6 Analysis of critical speed of rotor system

Figure 13 shows the Campbell diagrams for the three cases obtained from the numerical calculations: Fig. 13a is the Campbell diagram of the bearing-rotor system obtained without considering the seal, Fig. 13b is the Campbell diagram of the seal-bearing-rotor system obtained by considering the seal but neglecting the thermal deformation, and Fig. 13c is the Campbell diagram of the seal-bearing-rotor system obtained by considering the seal and thermal

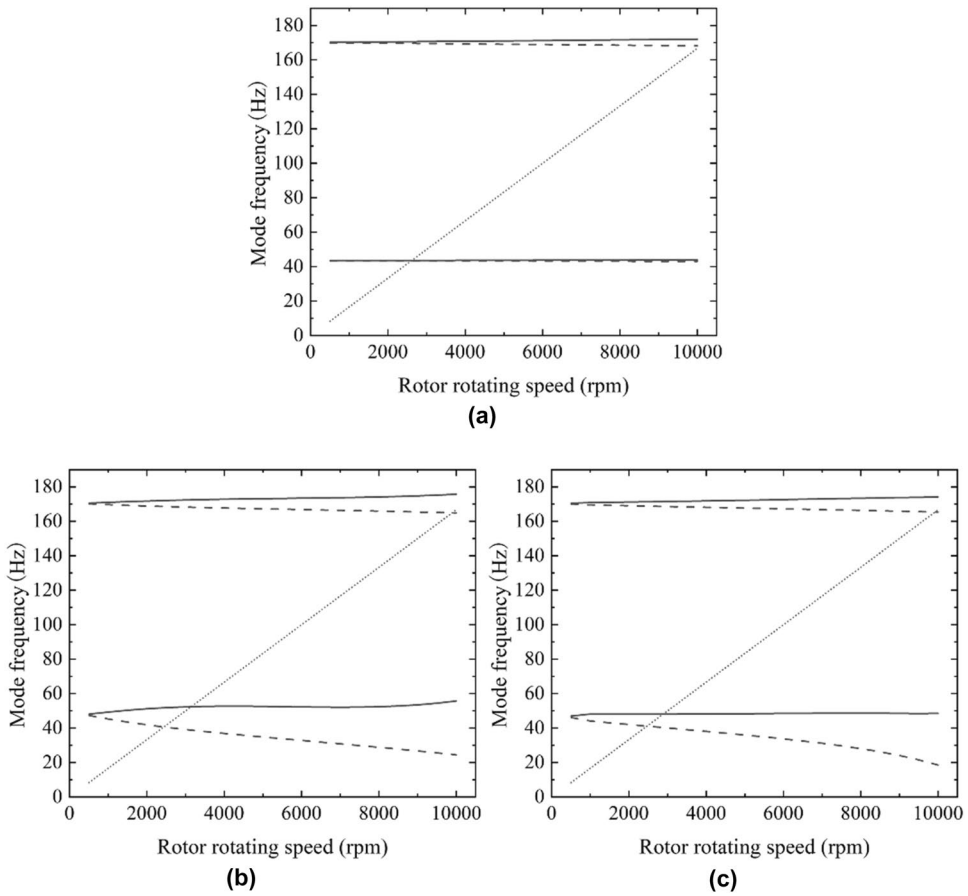


**Fig. 13** Campbell diagram of rotor system. **a** Without considering the seal; **b** considering the seal but neglecting the thermal deformation; **c** considering the seal and thermal deformation

deformation. The solid line represents the modal frequency of the forward motion, the dashed line represents the modal frequency of the reverse motion, and the dotted line represents the synchronous excitation line with a frequency equal to the speed. In engineering applications, only the modal frequency of the forward rotor motion is a major concern.

The comparison of Fig. 13a–c showed that the forward modal frequency of the rotor system of the molten salt pump obtained by considering the seal was larger than that obtained by neglecting the seal. This result shows that the presence of the seal makes the rotor system increase the frequency of each order of the forward motion mode; thus, the dynamic characteristics of the seal increase the rigidity of the rotor system and play a supporting role in ring location.

Table 3 shows the results of the first-order critical speed calculated for the three cases. Notably, the presence of the seal has a significant effect on the critical speed of the rotor of the molten salt pump. Among the three cases, the first-order critical speed is increased by 10.4% and 20.1% compared to 2615.6 rpm obtained by ignoring the seal, respectively, considering thermal deformation and neglecting thermal deformation. For the seal-bearing-rotor system, there is also a clear difference between the critical speed obtained by considering and neglecting the thermal deformation of the seal. Under the conditions of the high-temperature molten salt pump, thermal deformation occurs consequentially at the seal, and the corresponding seal dynamic characteristic coefficients are different. The calculated first-order critical speed of the rotor system was 2888.3 rpm. The operating speed of the high-temperature molten salt pump fulfills the requirements of the API610 standard, which can avoid self-excited vibrations during operation. Neglecting thermal deformation, the first-order critical speed of the rotor system was 3142 rpm. This is because the direct stiffness of the seal obtained by considering and neglecting the thermal deformation is different; therefore, the support effect on the rotor shaft is unequal. If

**Table 3** Comparison of first-order critical speed

| | Neglecting seal | Considering seal | |
|---|---|---|---|
| | | Neglecting thermal deformation | Considering thermal deformation |
| First-order critical speed (rpm) | 2615.6 | 3141.7 | 2888.3 |

the effect of seal thermal deformation in the actual operating conditions is neglected, the first-order critical speed of the rotor system will be overestimated, and the safety margin that remains for the speed will be overvalued, which introduces hidden dangers. Therefore, in the design of the rotor system of a high-temperature molten salt pump, the influence of the liquid film on the rotor system after the thermal deformation of the seal should be considered to better fulfill the actual working conditions and more accurately calculate the critical speed of the rotor system.

## 4 Conclusion

To study the leakage and dynamic characteristics of the liquid seal of a high-temperature molten salt pump in the molten salt medium, this study compared and analyzed the seal leakage, membrane pressure distribution, seal dynamic characteristics, seal stability, and critical speed of the rotor system under two cases: considering and neglecting thermal deformation. This study also discussed the influence of thermal deformation on the seal and suggested the necessity of research on seal thermal deformation. The main conclusions drawn are as follows:

1. After considering thermal deformation, seal clearance was reduced by 20.24%. At 1500 rpm of the molten salt pump, the difference in seal clearance leads to leakage at the seal ring, which differs by 38.2%. The leakage difference causes a discrepancy in the hydraulic performance of the pump in molten salt media, resulting in a significant deviation between the actual operating condition point and the design condition point.
2. The seal exhibited different dynamic characteristics after thermal deformation. When the pump shaft was at the operating speed, the difference in direct stiffness was 29.1%, and the difference in cross-coupled stiffness was 73.9%, representing the different support counterforces of the liquid film on the rotating shaft. The difference in direct damping was as high as 266.9%. The effective damping obtained by considering the thermal deformation is greater than that obtained by neglecting the thermal deformation of the seal; thus, the seal stability of the former is also better than that of the latter.
3. The presence of the seal not only increased the critical speed of the rotor system but also provided some damping to the rotor. The first-order critical speed obtained after the thermal deformation of the seal was less than that obtained by neglecting thermal deformation. Therefore, the difference should be considered in the design to ensure a sufficient safety margin such that the actual working condition of the pump rotor system fulfills the requirements of the API610 standard.

**Author contributions** All authors contributed to the study conception and design. Material preparation, data collection and analysis were performed by Xing-Chao Shen, Yuan Fu and Jian-Yu Zhang. The first draft of the manuscript was written by Xing-Chao Shen and all authors commented on previous versions of the manuscript. All authors read and approved the final manuscript.

## References

1. M.H. Jiang, H.J. Xu, Z.M. Dai, Advanced fission energy program-TMSR nuclear energy system. Bull. Chin. Acad. Sci. **27**(3), 366–374 (2012). https://doi.org/10.3969/j.issn.1000-3045.2012.03.016(inChinese)
2. J.A. Kocur, J.C. Nicholas, C.C. Lee, Surveying tilting pad journal bearing and gas labyrinth seal coefficients and their effect on rotor stability, in *Proceedings of the 36th Turbomachinery Symposium* (Texas A&M University, College Station, 2007). https://doi.org/10.21423/R16S83
3. H.F. Black, Effects of hydraulic force in annular pressure seals on the vibrations of centrifugal pump rotors. Mech. Eng. Sci. **11**, 206–213 (1969). https://doi.org/10.1243/JMES_JOUR_1969_011_025_02
4. D.W. Childs, Dynamic analysis of turbulent annular seals based on Hirs' lubrication equation. J. Lubr. Technol. **105**(3), 429–436 (1983). https://doi.org/10.1115/1.3254633
5. J.J. Moore, A.B. Palazzolo, CFD comparison to 3D laser anemometer and rotordynamic force measurements for grooved liquid annular seals. J. Tribol. **121**(2), 306–314 (1999). https://doi.org/10.1115/1.2833937
6. A. Untaroiu, V. Hayrapetian, C.D. Untaroiu et al., On the dynamic properties of pump liquid seals. J. Fluids Eng. **135**(5), 51–104 (2013). https://doi.org/10.1115/1.4023653
7. M. Daqiqshirazi, R. Torabi, A. Riasi et al., The effect of wear ring clearance on flow field in the impeller sidewall gap and efficiency of a low specific speed centrifugal pump. Proc. Inst. Mech. Eng. Part C **232**(17), 3062–3073 (2017). https://doi.org/10.1177/0954406217729420
8. C.L. Shao, J.F. Zhou, W.J. Cheng, Effect of viscosity on the external characteristics and flow field of a molten salt pump in the view of energy loss. Heat Mass Transf. **55**(3), 711–722 (2019). https://doi.org/10.1007/s00231-018-2450-z
9. K. Wang, X. Lu, Y. Li et al., Performance improvement of a liquid molten salt pump: geometry optimization and experimental verification. Symmetry **11**(3), 423 (2019). https://doi.org/10.3390/sym11030423
10. H. He, *Effect of Wear Ring Clearance on the Performance of Molten Salt Pump and the Force, Deformation of Rotor* (Power Engineering, Lanzhou University of Technology, 2019)
11. Y.Y. Hu, D.Z. Wang, Y. Fu et al., Numerical study on rotordynamic coefficients of the seal of molten salt pump. Nucl. Sci. Tech. **27**(5), 114 (2016). https://doi.org/10.1007/s41365-016-0116-4
12. S. Subramanian, A.S. Sekhar, B.V.S.S.S. Prasad, Influence of combined radial location and growth on the leakage performance of a rotating labyrinth gas turbine seal. J. Mech. Sci. Technol. **29**, 2535–2545 (2015). https://doi.org/10.1007/s12206-015-0545-8
13. S. Subramanian, A.S. Sekhar, B.V.S.S.S. Prasad, Rotordynamic characterization of rotating labyrinth gas turbine seals with radial growth: combined centrifugal and thermal effects. Int. J. Mech. Sci. **123**, 1–19 (2017). https://doi.org/10.1016/j.ijmecsci.2017.01.033
14. J. Chen, X.Y. Jiang, L.C. Lin et al., Optimization for surface texture on the shaft sleeve of a high temperature molten salt pump in molten salt reactor. Nucl. Technol. **42**, 050602 (2019). https://doi.org/10.11889/j.0253-3219.2019.hjs.42.050602. (**in Chinese**)

15. Y. Zhu, J.L. Yin, J.G. Zhang et al., Pressure fluctuation at inlet and outlet of the canned nuclear coolant pump. Nucl. Tech. **36**, 110601 (2013). https://doi.org/10.11889/j.0253-3219.2013.hjs.36.110601. (**in Chinese**)
16. Y. Wang, J. Tian, S.W. Wang et al., Experimental study on the penetration characteristics of leaking molten salt in the thermal insulation layer of aluminum silicate fiber. Nucl. Sci. Tech. **32**(9), 92 (2021). https://doi.org/10.1007/s41365-021-00935-6
17. A. Picardo, D.W. Childs, Rotordynamic coefficients for a tooth-on-stator labyrinth seal at 70 bar supply pressures: measurements versus theory and comparisons to a hole-pattern stator seal. J. Eng. Gas Turbines Power **127**, 843–855 (2005). https://doi.org/10.1115/1.1924634
18. N.G. Wagner, K. Steff, R. Gausmann et al., Investigations on the dynamic coefficients of impeller eye labyrinth seals, in *Proceedings of the 38th Turbomachinery Symposium* (Texas A&M University. Turbomachinery Laboratories, 2009), pp. 53–70. https://doi.org/10.21423/R18061
19. W.T. Lindsey, D.W. Childs, The effects of converging and diverging axial taper on the rotordynamic coefficients of liquid annular pressure seals: theory versus experiment. J. Vib. Acoust. **122**, 126–131 (2000). https://doi.org/10.1115/1.568457
20. Z.S. Xu, *The Mechanism and Simulation Research on Thermal Deformation of Mechanical Parts* (Instrument Engineering, Hefei University of Technology, 2015)
21. Y. Ni, *Research on Functional Dimensions of Mechanical Hole and Shaft Parts* (Measuring Technology and Instruments, Hefei University of Technology, 2016)
22. E.M. Miao, Z.S. Xu, X.S. Zhou et al., Simulation of thermal deformation of cylindrical mechanical parts bounded by boundary constraint based on conversion mechanism of thermal into mechanics. Opt. Precis. Eng. **23**(2), 504–510 (2015). https://doi.org/10.3788/OPE.20152302.0504(inChinese)